Physicochem. Probl. Miner. Process., 56(3), 2020, 449-459

http://www.journalssystem.com/ppmp

Physicochemical Problems of Mineral Processing

ISSN 1643-1049

Received December 28, 2019; reviewed; accepted March 09, 2020

Effect of particle size on reduction kinetics of hematite ore in suspension roaster

Peng Gaob [1], Yaxiong An [1], Guofeng Li [2], Yuexin Han [1]

[1] College of Resources and Civil Engineering, Northeastern University, Shenyang 110819, China

[2] College of Mining Engineering, North China University of Science and Technology, Tangshan 063210, China

Corresponding author: liguofengncu@sina.com (Guofeng Li)

Abstract: Suspension magnetization roasting followed by magnetic separation is an innovative and effective way to recover iron from refractory iron ores, and the particle size of the ore greatly affects the roasting index. To identify the effect of particle size on the reduction kinetics for the transformation of hematite to magnetite, a high-purity hematite ore with different size fractions were isothermally reduced using a suspension roaster. The pure hematite ore was divided into -1000+500 μm, -500+150 μm, -150+74 μm, -74+37 μm and -37 μm size fractions, while the gas mixture of CO and CO_2 with a volume ratio of 1:4 was used as reductant. The results showed that the most suitable mechanism function for the reduction of -37 μm size fraction hematite ore is the Avrami-Erofeev model. In the case of -500+37 μm size fraction, the reduction process can be described by first-order chemical reaction model. For -1000+500 μm size fraction, the reduction of hematite ore is restricted by the second-order chemical reaction. In addition, scanning electron microscopy (SEM) analysis results demonstrated that the transformation of hematite particles to magnetite is in accordance with the characteristics of shrinking core model. The phase transformation primarily occurs at the edge of hematite particles and then develop towards the inner side of particles. The findings of this paper provide a theoretical basis for the development and utilization of refractory hematite ore via suspension magnetization roasting technology.

Keywords: hematite, suspension magnetization roasting, particle size, reduction kinetics

1. Introduction

The rapid development of world economy results in the requirement for a large quantity of ore resources, especially iron ore resources (Li et al. 2016; Sun et al., 2019). With the depletion of high-quality iron ores, the utilization of refractory iron ores, such as fine-grain disseminated hematite, siderite, limonite, and oolitic hematite ores, has received increased attention (Feilmayr et al., 2004; Li et al., 2015; Yu et al., 2017). The explored reserves of those iron ores reach 20 billion tons in China, which is characterized by complex mineral composition and ultra-fine grain size of iron minerals. It is difficult to enrich iron minerals of refractory iron ores using conventional fine grinding followed by forth flotation or magnetic separation effectively (Nunes et al., 2012; Gao et al., 2016; Zhu et al., 2019).

Magnetization roasting, including rotary kiln magnetization roasting, shaft furnace magnetization roasting, and suspension magnetization roasting, is regarded as an effective method to treat refractory iron ores (Yu et al., 2018a). Among them, suspension magnetization roasting has obvious advantages in terms of full gas-solid contact, high mass transfer and heat transfer efficiency, and low roasting energy consumption. The suspension magnetization roasting of iron ores are carried out at suspension roaster, which usually consists of gas supply system, reaction equipment, and control system (Li et al., 2019; Sun et al., 2019). The suspension magnetization roasting has become a research hotspot in processing field of refractory iron ores (Li et al., 2010; Yang et al., 2011; Chun et al., 2015; Li et al., 2018). A refractory iron ore comprising hematite, siderite, and gangue minerals was separated by Zhang et al. (2019) using

DOI: 10.37190/ppmp/118841

suspension magnetization roasting followed by magnetic separation technology, and the results showed that the iron grade and recovery increased by 12–14% and 17–22%, respectively, comparing with shaft furnace magnetization roasting method. Gao et al. (2019) proposed a pressure drop model aiming to predict the pressure of reduction chamber during the suspension magnetization roasting process of iron ores. Tang et al. (2019) investigated the fluidization characteristics of particles in reduction chamber of suspension roaster and found that fluidization velocity was seriously affected by particle size and the aeration velocity.

To exploit magnetization roasting mechanism of iron ores, many researches were conducted. It was reported that the type of reducing agents greatly affected the reduction of iron oxides, and the activity of reducing gases decreased in the sequence of H_2, CH_4, CO, and generator gas (Zenkov and Pasichnyi, 2010). Yu et al. (2018b) analyzed the phase transformation behavior of hematite and siderite in the magnetic preconcentrate of an iron ore tailing during roasting process. The results revealed that most of the hematite and siderite were reduced to magnetite apart from a bit of magnetite-hematite interlocking particles. Jang et al. (2014) reported that the goethite could be converted to hematite and eventually magnetite after reduction roasting. Et-tabirou et al. (1988) studied the effect of roasting temperature on the nucleation of reduced hematite and the morphology of new produced magnetite using CO as a reductant. The results showed that the new produced magnetite presented dense massive or needle-like structure at > 1273°K. However, the microcracks generated in the hematite particles at temperatures ranging from 673°K to 1073°K. The new produced magnetite exhibited porous shape because the magnetite was easy to nucleate and growth at the cracks. Similar results were obtained by Swann and Tighe (1977). They observed the dense massive or needle-like structure magnetite at > 1073°K and honeycomb porous structure magnetite at < 923°K. Meanwhile, the magnetite with two-types structure mentioned above were detected when temperatures ranging from 923°K to 1073°K. Hou et al. (2012) investigated the reduction kinetics of hematite in suspension magnetization roasting process, and determined that the apparent activation energy and the pre-exponential factor were 105.4 kJ/mol and 4.6×10^4 s^{-1}, respectively, at 713°K to 763°K temperatures with the mixed gas of H_2 and Ar as a reductant. Although the particle size has been proved to be an important factor affecting the fluidization velocity, which will further affect the roasting index of refractory iron ores, the corresponding researches have not been reported so far.

In this paper, a high-purity hematite ore was divided into different size fractions. Every size fraction was isothermally reduced by suspension magnetization roasting, and the corresponding reduction kinetics was studied. Then, the effect of particle size on suspension magnetization roasting behavior of hematite was analyzed. Finally, the reduction process of hematite was investigated. The results of this research will provide a theoretical support for the suspension magnetization roasting of refractory iron ores.

2. Materials and methods

2.1. Materials

The hematite ore with a purity of 92.47 wt.% collected from Hainan, China was crushed to 100% passing 1000 mm. The ore sample contains 64.73 wt.% total iron and a small amount of impurities, including 2.12 wt.% SiO_2, 1.27 wt.% Al_2O_3, 0.21 wt.% CaO, and 0.26 wt.% MgO. The X-ray diffraction analysis (PANalytical X'pert PW3040) result further indicates that the main mineral of the ore sample is hematite (Fig.1).

Prior to use, the hematite ore was divided into -1000+500 μm, -500+150 μm, -150+74 μm, -74+37 μm and -37 μm size fractions. In addition, the mixed gas of CO and CO_2 with a volume ratio of 1:4 was used as reductant. The purity of CO and CO_2 was 99.99%.

2.2. Experimental equipment and method

As schematically illustrated in Fig. 2, the suspension roaster is mainly divided into two parts, gas supply system and roasting device. In gas supply system, the gas flow is quantitatively controlled by proton flowmeter combining with a pressure valve of gas collecting cylinder. Meanwhile, the KSL-1200x

vertical tube furnace, produced by Hefei Kejing Material Technology Co. Ltd., is used for suspension magnetization roasting. The maximum heating rate of the furnace is 15°K/min.

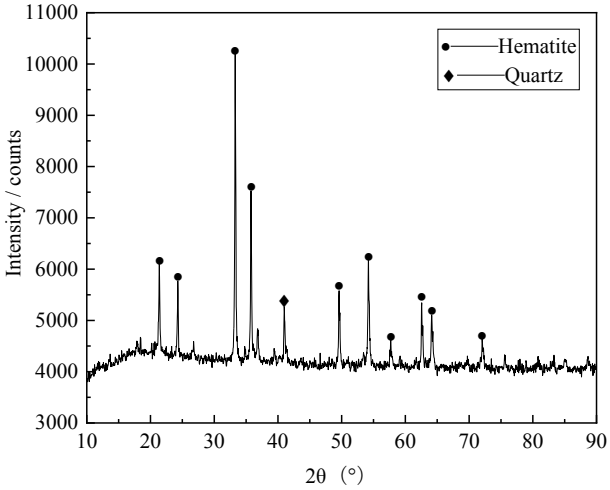

Fig. 1. XRD image of the ore sample

According to the explored results of cold test, the gas flow rate of 800 ml/min can guarantee the suspension state of hematite particles with different size fractions. Therefore, the N_2 with a flow rate of 800 ml/min was introduced to discharge the air from the furnace tube after placing ore sample in it. The temperature of furnace tube was increased to 753, 793, 833 or 873°K with a heating rate of 15°K/min. The magnetization roasting was then conducted by replacing N_2 with same flow rate mixed reducing gas. After roasting, the products were cooled to room temperature with the protection of N_2 and taken out from the furnace tube. The FeO content of the products was determined by chemical analysis.

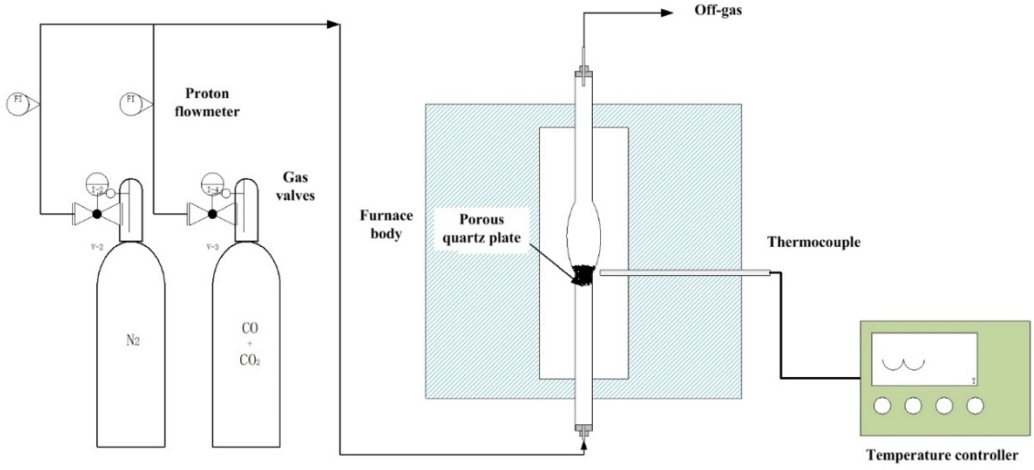

Fig. 2. Schematic diagram of suspension roaster

2.3. Mechanism function determination method

To m g hematite ore with a purity of ε, the quality of hematite and impurities are $m \cdot \varepsilon$ and $m \cdot (1-\varepsilon)$, respectively. The conversion rate of hematite to magnetite after t minutes roasting is defined as α. Therefore, the following relationship will be existed (Yu et al., 2019):

$$\begin{matrix} 3\,Fe_2O_3(s) + CO(g) = 2Fe_3O_4(s) + CO_2(g) \\ 3\times160 \qquad\qquad 2\times232 \\ m\cdot\varepsilon\cdot\alpha \qquad\qquad M_{Fe_3O_4} \end{matrix} \tag{1}$$

Given that the Fe_3O_4 can be rewritten to $Fe_2O_3 \cdot FeO$, the quality of new produced magnetite and FeO can be given by Eqs. (2) and (3).

$$M_{\mathrm{Fe_3O_4}}=\frac{2\times232}{3\times160}\cdot m\cdot\varepsilon\cdot\alpha \tag{2}$$

$$M_{\mathrm{FeO}}=\frac{72}{232}\cdot M_{\mathrm{Fe_3O_4}}=0.3\cdot m\cdot\varepsilon\cdot\alpha \tag{3}$$

The quality of unreduced hematite and impurities in products can be generally represented by Eqs. (4) and (5):

$$M_{\mathrm{Fe_2O_3}}=m\cdot\varepsilon\cdot(1-\alpha) \tag{4}$$

$$M_{\mathrm{Impurity}}=m\cdot(1-\varepsilon) \tag{5}$$

The FeO content of roasting products (ω_{FeO}) can be expressed as:

$$\omega_{\mathrm{FeO}}=\frac{M_{\mathrm{FeO}}}{M_{\mathrm{Fe_2O_3}}+M_{\mathrm{Fe_3O_4}}+M_{\mathrm{Impurity}}}=\frac{9\cdot\varepsilon\cdot\alpha}{30-\varepsilon\cdot\alpha} \tag{6}$$

Therefore, the conversion rate α can be calculated by:

$$\alpha=\frac{30\cdot\omega_{\mathrm{FeO}}}{(9+\omega_{\mathrm{FeO}})\cdot\varepsilon} \tag{7}$$

The conversion rate and roasting time values were then submitting into Eq. (8), which was usually used for characterizing the kinetics of gas-solid reactions (Vyazovkin et al., 2011; Wang et al., 2016; Li et al., 2017). A trial-and-error method was used to determine the most suitable mechanism function.

$$G(\alpha)=\int_0^t k(T)dt=k(T)t \tag{8}$$

where $G(\alpha)$ is the mechanism function, $k(T)$ is the apparent reaction rate constant, min^{-1}, t is the roasting time, min.

2.4. Roasting products analysis

The products produced at 833°K and after 1, 2, 4, and 10 min roasting were investigated using Hitachi S-3400N scanning electron microscope (SEM) equipped with an energy dispersive spectroscope (EDS). The acceleration voltage was 20 kV. According to the small color difference, the images of the roasted particles were divided into two zones. To exhibit it clear, we separated the different zones of the images using red line. The exist areas of hematite and magnetite were then determined combining with EDS analysis. Meanwhile, the phase transition behavior of hematite to magnetite during roasting process was analyzed.

3. Results and discussion

3.1. Conversion rate analysis

The conversion rate of hematite was calculated by substituting the purity of hematite ore and FeO content of the products obtained during the roasting process into Eq. (7). The conversion rate of hematite as a function of roasting time is shown in Fig. 3.

It can be seen from Fig. 3(a) that the conversion rate of hematite increased with extending roasting time or increasing roasting temperature for -37 μm size fraction. For example, the convention rate of hematite rapidly increased from 8.81 wt.% to 95.89 wt.% with roasting time extending from 0.5 min to 10 min and slowly increased to 97.33 wt.% after 12 min roasting at 753°K. Meanwhile, the convention rate of hematite jumped to 83.09 wt.% from 48.84% at a roasting time of 4 min when the roasting temperature climbed from 753°K to 873°K. The similar phenomenon was exhibited by the conversion rate curves of other size fractions.

The conversion rate of hematite was also observed to be greatly affected by the particle size of the ore sample from Fig. 3(a)~(e). A coarser size fraction led to a longer roasting time and a lower conversion rate. The conversion rate of hematite was close to 100 wt.% after 12 min roasting for -37 μm size fraction while it was 86.50 wt.% after 18 min roasting for -1000+500 μm size fraction at 753°K.

3.2. Mechanism function determination

The conversion rate and time data in Fig. 3 were fitted into Eq. (8), and the most suitable mechanism function gave a maximum value of correlation coefficient. The commonly used mechanism functions

$G(\alpha)$ and the corresponding average correlation coefficient of different size fractions reduced at 753, 793, 833, and 873°K are listed in Table 1.

As shown in Table 1, the most suitable mechanism functions for -1000+500 μm, -500+37 μm, and -37 μm size fraction were $G(\alpha) = (1-\alpha)^{-1} - 1$, $G(\alpha) = -\ln(1-\alpha)$, and $G(\alpha) = [-\ln(1-\alpha)]^{1/3}$, respectively. Fig. 4 shows the relation between $G(\alpha)$ and roasting time for different size fractions under four temperature conditions. The corresponding apparent reaction rate constant and mechanism are summarized in Table 2.

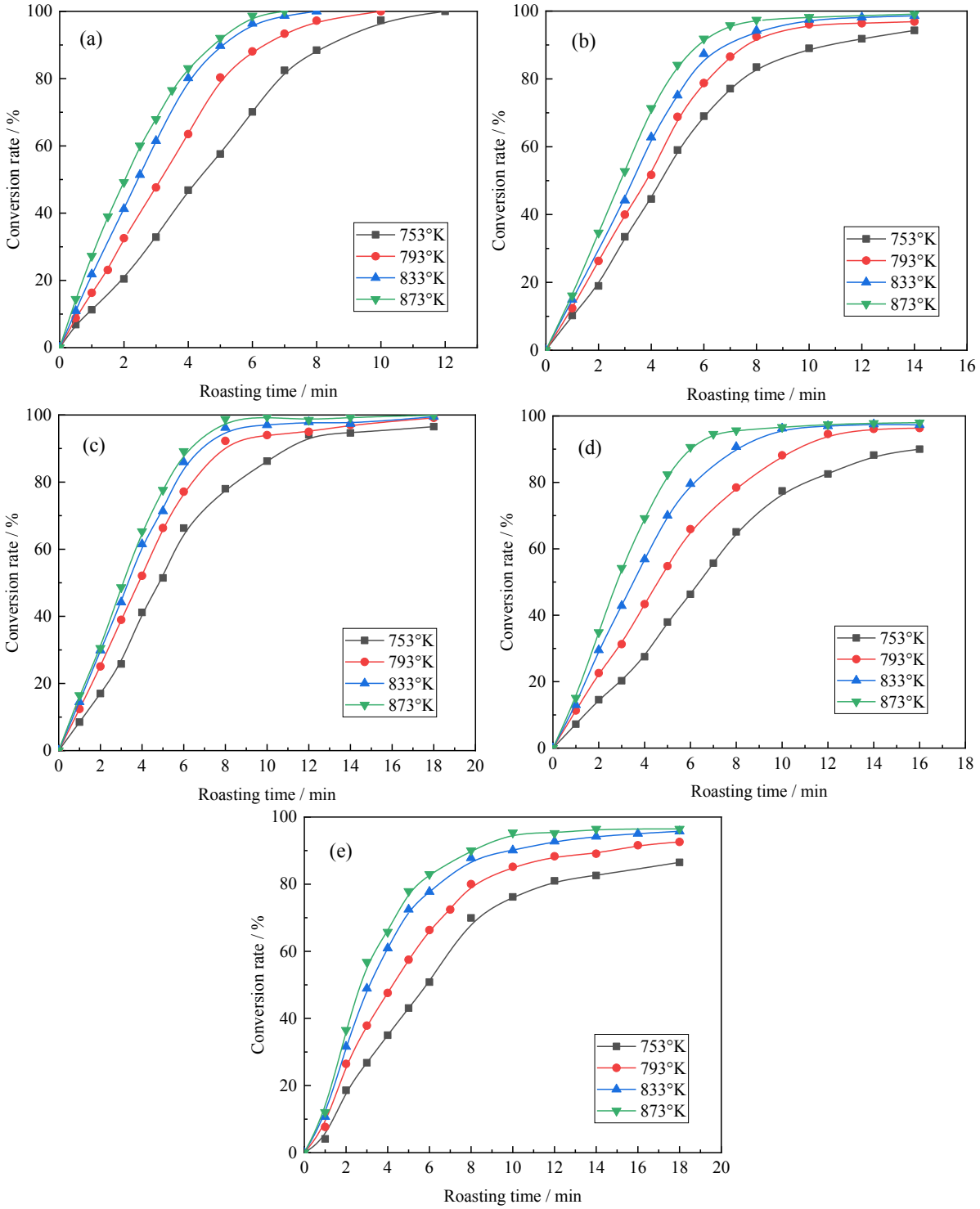

Fig. 3. Effect of particle size and temperature on convention rate of hematite: (a) -37 μm size fraction, (b) -74+37 μm size fraction, (c) -150+74 μm size fraction, (d) -500+150 μm size fractio, (e) -1000+500 μm size fraction

Table 1. Fitting analysis results of commonly used kinetic mechanism functions

number	Mechanism function $G(\alpha)$	Average correlation coefficient R^2				
		-37 μm	-74+37 μm	-150+74 μm	-500+150 μm	-1000+500 μm
A2	$[-\ln(1-\alpha)]^{1/2}$	0.9947	0.9251	0.9141	0.9450	0.8695
A3	$[-\ln(1-\alpha)]^{1/3}$	0.9956	0.8915	0.8852	0.9232	0.8258
A4	$[-\ln(1-\alpha)]^{1/4}$	0.9906	0.8739	0.8672	0.9087	0.7996
A3/2	$[-\ln(1-\alpha)]^{2/3}$	0.9814	0.9405	0.9394	0.9580	0.9023
A1/4	$[-\ln(1-\alpha)]^{4}$	0.5160	0.8607	0.7726	0.8093	0.9134
A1/3	$[-\ln(1-\alpha)]^{3}$	0.5995	0.9055	0.8324	0.8588	0.9466
A1/2	$[-\ln(1-\alpha)]^{2}$	0.7362	0.9491	0.9199	0.9175	0.9675
R1/2	$1-(1-\alpha)^{2}$	0.7631	0.5987	0.5708	0.6973	0.5707
R1/3	$1-(1-\alpha)^{3}$	0.6505	0.4918	0.4659	0.5855	0.4440
R1/4	$1-(1-\alpha)^{4}$	0.5712	0.4237	0.3986	0.5072	0.3621
R2	$1-(1-\alpha)^{1/2}$	0.9951	0.8836	0.8599	0.9265	0.8777
R3	$1-(1-\alpha)^{1/3}$	0.9776	0.9159	0.8983	0.9448	0.8949
R4	$1-(1-\alpha)^{1/4}$	0.9324	0.9302	0.9160	0.9520	0.9087
D1	α^{2}	0.9629	0.8465	0.8143	0.9029	0.8570
D2	$\alpha+(1-\alpha)\ln(1-\alpha)$	0.9713	0.8973	0.8669	0.9281	0.9073
D3	$[1-(1-\alpha)]^{1/2}]^{2}$	0.9408	0.9319	0.9111	0.9394	0.9370
D4	$[(1+\alpha)]^{1/3}-1]^{2}$	0.9546	0.8251	0.7934	0.8899	0.8306
D5	$[(1-\alpha)]^{-1/3}-1]^{2}$	0.5836	0.9029	0.7493	0.8712	0.9551
D6	$[1-(1-\alpha)]^{1/3}]^{2}$	0.8404	0.9483	0.9356	0.9393	0.9538
D7	$[1-(1-\alpha)]^{1/3}]^{1/2}$	0.9927	0.8558	0.8378	0.9026	0.8071
D8	$1-2/3\alpha-(1-\alpha)^{2/3}$	0.9631	0.9202	0.8950	0.9363	0.9272
P4	$\alpha^{1/4}$	0.8223	0.6724	0.6439	0.7405	0.6069
P3	$\alpha^{1/3}$	0.8374	0.6860	0.6575	0.7651	0.6282
P2	$\alpha^{1/2}$	0.8646	0.7117	0.6828	0.7919	0.6679
P1	α	0.9226	0.7747	0.7442	0.8515	0.7603
P3/2	$\alpha^{3/2}$	0.9519	0.8180	0.7863	0.8857	0.8193
F1	$-\ln(1-\alpha)$	0.9298	0.9619	0.9565	0.9710	0.9427
F2	$(1-\alpha)^{-1}-1$	0.5835	0.9053	0.7116	0.8936	0.9676
F3	$(1-\alpha)^{-2}$	0.4217	0.7658	0.5361	0.7698	0.8695

As shown in Table 2, the particle size affected the transformation behavior of hematite to magnetite during roasting process. For -37 μm size fraction, the reduction of hematite could be described by Avrami-Erofeev model, namely the transformation process was controlled by the nucleation and growth of magnetite. However, it was restricted by first-order and second-order chemical reaction when

the size fractions were -500+37 μm and -1000+500 μm, respectively. This phenomenon maybe attribute to the fact that the reduced reaction carried out from the edge to the inner side of hematite particles. For fine particles, the hematite was easy to be reduced because the sufficient contact of reduced gas and hematite. In the case of coarse particles, the contact of hematite particles' inner sides with reduced gas became more difficult, which slowed the reaction rate.

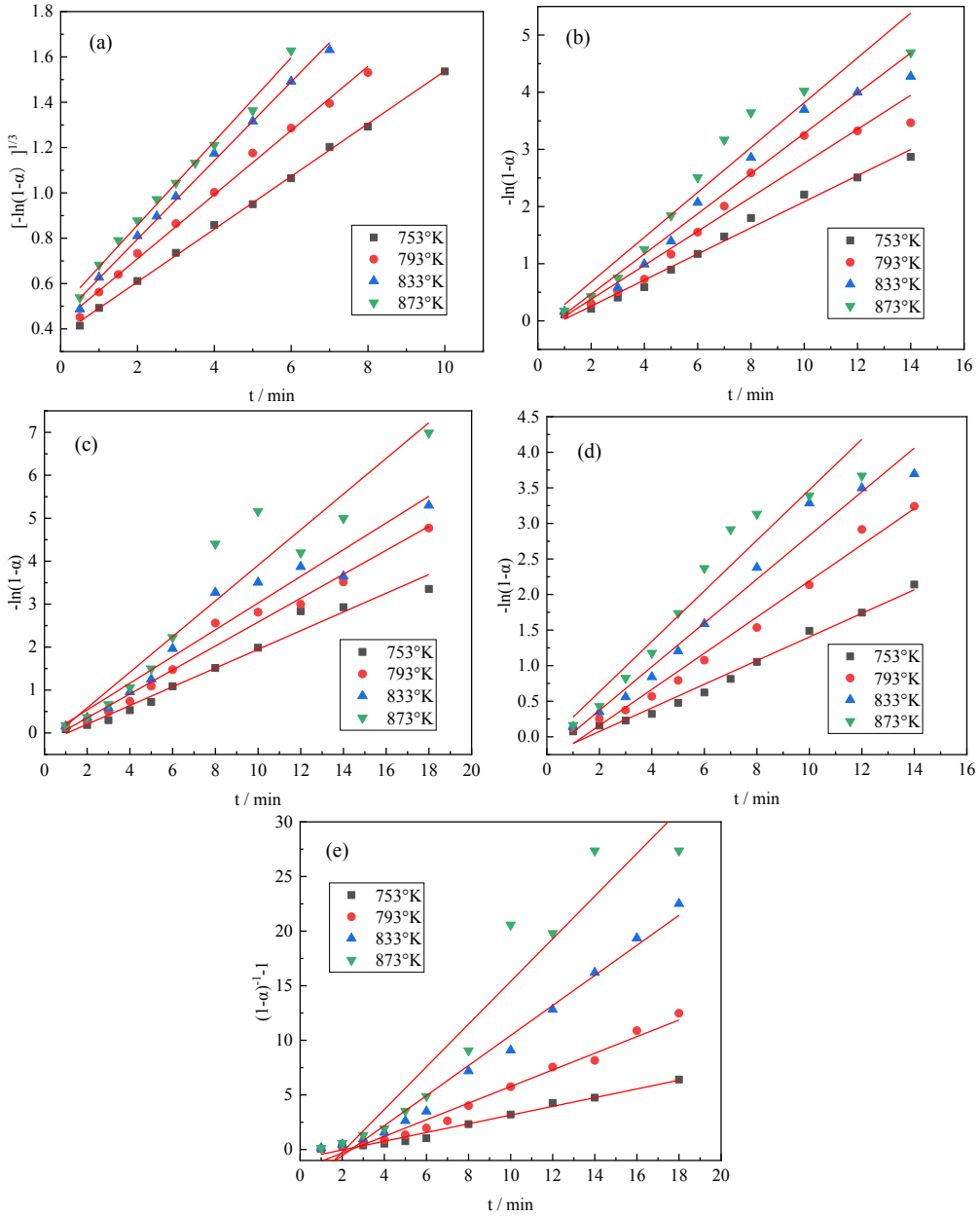

Fig. 4. Linear fitting of $G(\alpha)$ versus t at different temperatures: (a) -37 μm size fraction; (b) -74+37 μm size fraction; (c) -150+74 μm size fraction; (d) -500+150 μm size fraction; (e) -1000+500 μm size fraction

3.3. Kinetic parameters determination

All apparent reaction rate and temperature values in terms of different size fractions were fitted into the Arrhenius function, which is expressed as follows:

$$\ln k = \ln A - \frac{E_\alpha}{R} \cdot \frac{1}{T} \tag{9}$$

where A is the pre-exponential factor, min^{-1}; E_α is the apparent activation energy, $J \cdot mol^{-1}$; R is the universal gas constant, 8.314 $J \cdot mol^{-1} \cdot °K^{-1}$. T is the roasting temperature, °K.

Fig. 5 shows the linear fitting of $\ln k$ versus $1/T$ for different size fractions. The fitted curves exhibited a good linear with the values of correlation coefficient all above 0.95. The apparent activation energy and pre-exponential factor calculated for the reduced reaction are listed in Table 3.

Table 2. The apparent reaction rate and mechanism for different size fractions

Size fraction	Apparent reaction rate k/min^{-1}				Mechanism function $G(\alpha)$	Mechanism
	753°K	793°K	833°K	873°K		
-37 μm	0.3740	0.4267	0.4491	0.4886	$[-\ln(1-\alpha)]^{1/3}$	Avrami-Erofeev model
-74+37 μm	0.2285	0.2975	0.3516	0.3923	$-\ln(1-\alpha)$	First-order chemical reaction
-150+74 μm	0.2179	0.2787	0.3110	0.4149	$-\ln(1-\alpha)$	First-order chemical reaction
-500+150 μm	0.1661	0.2541	0.3074	0.3550	$-\ln(1-\alpha)$	First-order chemical reaction
-1000+500 μm	0.3992	0.9772	0.9819	0.9296	$(1-\alpha)^{-1}-1$	Second-order chemical reaction

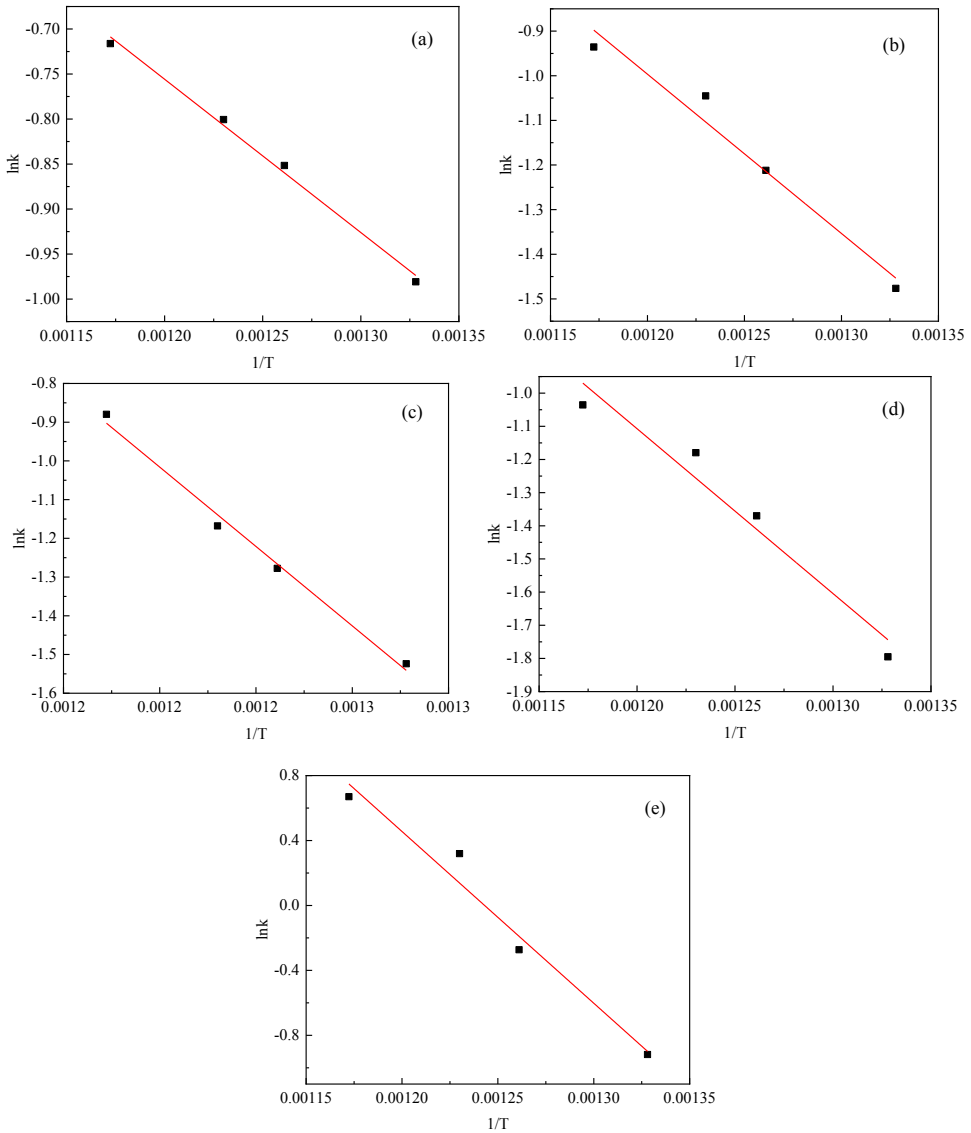

Fig. 5. Linear fitting of $\ln k$ versus $1/T$ for magnetization roasting of hematite particles: (a) -37 μm size fraction; (b) -74+37 μm size fraction; (c) -150+74 μm size fraction; (d) -500+150 μm size fraction; (e) -1000+500 μm size fraction

Table 3. Kinetic parameters of the magnetization roasting of hematite particles

Size fraction	Apparent activation energy E_α/ kJ·mol^{-1}	Pre-exponential factor A/ min^{-1}
-37 μm	14.16	3.62
-74+37 μm	29.67	26.73
-150+74 μm	34.08	49.57
-500+150 μm	41.32	128.64
-1000+500 μm	87.94	513322.71

As seen in Table 3, a coarser particle size resulted in a higher apparent activation energy and pre-exponential factor. The apparent activation energy and pre-exponential factor were 14.16 kJ·mol^{-1} and 3.62 min^{-1} at -37 μm size fraction while they increased from 29.67 kJ·mol^{-1} and 26.73 min^{-1} to 41.32 kJ·mol^{-1} and 128.64 min^{-1}, respectively, with increasing size fraction from -74+37 μm to -500+150 μm. When the particle size was increased to -1000+500 μm, the apparent activation energy and pre-exponential factor jumped to 87.94 kJ·mol^{-1} and 513322.71 min^{-1}, respectively. This is because a coarser particle size increased the thickness of new generated magnetite layer, which increased the diffusion resistance of reduced gas to the reaction interface and decreased the gas concentration of reaction interface. Therefore, the minimum energy needed for reduced reaction increased with increasing particle size. Meanwhile, the effective collision between reduced gas and hematite molecules decreased at reaction interface, and a higher collision frequency was required to guarantee the full reduced reaction.

3.4. Reduction process analysis

Taking -74+37 μm size fraction of hematite ore into account, the roasting products produced at 833°K and different roasting time were analyzed to clarify the reduction process of hematite. The SEM images of the roasting products are shown in Fig. 6.

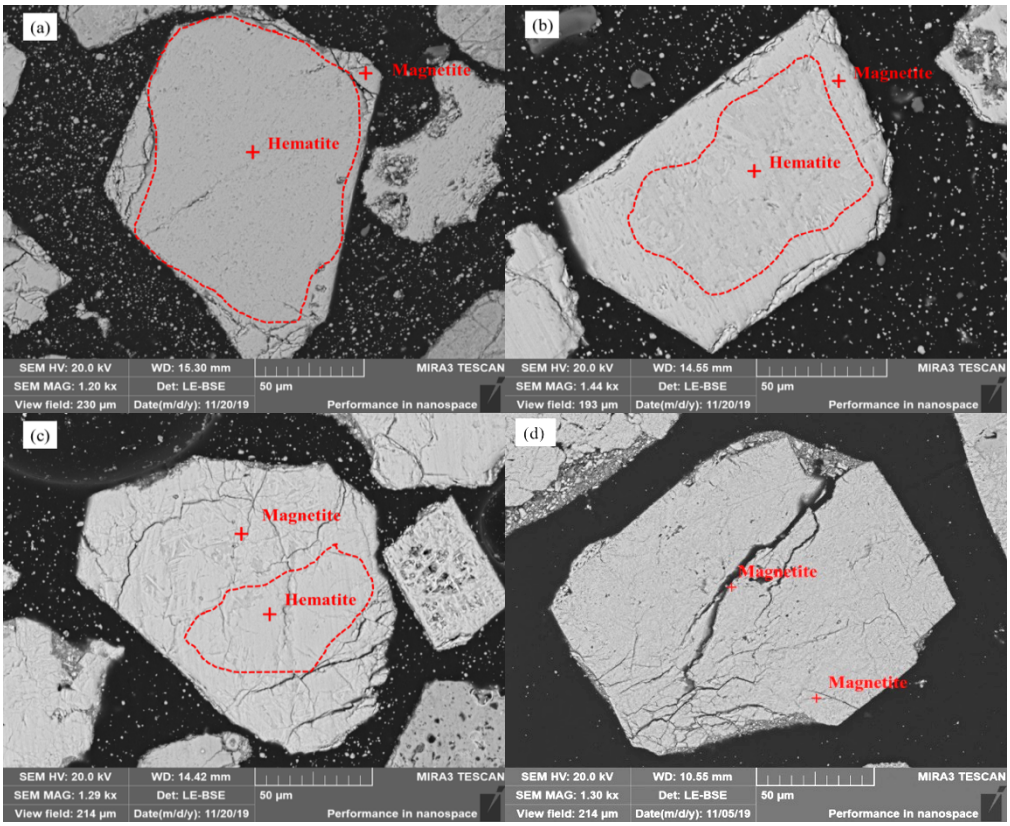

Fig. 6. SEM images of roasting products produced at different times: (a) 1 min; (b) 2 min; (c) 4 min; (d) 10 min

It can be seen that a small amount of hematite was reduced to magnetite at the edge of the particles within 1 min roasting (Fig. 6a). When the roasting time was extended to 2 or 4 min, more hematite was transformed to magnetite (Fig. 6b, c). The hematite area of the particles decreased significantly, and the layer of new produced magnetite became thicker. At the roasting time of 10 min, the hematite was almost completely converted into magnetite (Fig. 6d).

All in all, the reduction process of hematite particles exhibited the characteristics of shrinking core model. At the initial stage of the roasting, the phase transformation occurred at the edge of particles and quickly reacted towards the inner side of the particles. With the proceeding of the reaction, the increased layer thickness of new produced magnetite led to an increased diffusion resistance of reduced gas, which resulted in a gradually decreased reaction rate. The above results further verify the deduction in section 3.2 and 3.3.

4. Conclusions

A high-purity hematite ore was magnetization roasted using the mixed gas of CO and CO_2 as a reductant. The effect of particle size on the reduction behavior, especially the reduction kinetics, of hematite ore was analyzed in detail. According to the present investigation, the following conclusions can be drawn.

A higher temperature and a longer roasting time gave a higher conversion rate of hematite to magnetite. The particle size greatly affected the roasting behavior of hematite. The roasting time was prolonged, but the conversion rate was decreased with increasing particle size.

The restriction factors were dissimilar for the roasting process of hematite in terms of different particle size. The roasting process of -37 μm, -500+37 μm, and -1000+500 μm size fractions were restricted by nucleation and growth of magnetite, first-order chemical reaction, and second-order chemical reaction, respectively.

The apparent activation energy and pre-exponential factor of reduced reaction increased with increasing particle size. The apparent activation energy and pre-exponential factor were 14.16 kJ·mol^{-1} and 3.62 min^{-1} for -37 μm size fraction, whereas those were 87.94 kJ·mol^{-1} and 513322.71 min^{-1}, respectively, for -1000+500 μm size fraction.

The phase transformation of hematite to magnetite during the roasting process was in accordance with the characteristics of shrinking core model. The reduced reaction firstly occurred at the edge and proceeded towards the inner side of the particles. The distinction of the layer thickness of new produced magnetite resulted from different particle size significantly affected the diffusion of reduced gas, which was also the major cause affecting the reduction kinetics of hematite during the roasting process.

Acknowledgments

The authors gratefully acknowledge the National Natural Science Foundation of China (Grant No. 51674064, 51674065, and 51734005) for funding this research.

References

CHUN, T. J., ZHU D. Q., PAN J., 2015. *Simultaneously roasting and magnetic separation to treat low grade siderite and hematite ores*. Min. Proce. Ext. Met. Rev. 36, 223-226.

ET-TABIRON, M., DUPRE, B., GLEITZER, C., 1988. *Hematite single crystal reduction into magnetite with CO-CO_2*. Metall. Mater. Trans. B 19, 311-317.

FEILMAYR, C., THURNHOFER, A., WINTER, F., 2004. *Reduction behavior of hematite to magnetite under fluidized bed conditions*. ISIJ Int. 44, 1125-1133.

GAO, P., LI, G. F., HAN, Y. X., SUN, Y. S., 2016. *Reaction behavior of phosphorus in coal-based reduction of an oolitic hematite ore and pre-dephosphorization of reduced iron*. Metals 6, 82.

GAO, P., Tang, Z., HAN, Y., LI, E., ZHANG, X., 2019. *A pressure drop model of u-typed reduction chamber for iron ore suspension roasting*. Powder Technol. 343, 255-261.

HAN, Y. X., LI, G. F., GAO, P., SUN, Y. S., 2017. *Reduction behaviour of apatite in oolitic haematite ore using coal as a reductant*. Ironmak. Steelmak. 44, 287-293.

HOU, B. L., ZHANG, H. Y., LI, H. Z., 2012. *Study on kinetics of iron oxide reduction by hydrogen*. Chinese J. Chem. Eng. 20, 10-17.

JANG, K., NUNNA, V., HAPUGODA, S., NGUYEN, A., BRUCKARD, W., 2014. *Chemical and mineral transformation of a low grade goethite ore by dehydroxylation, reduction roasting and magnetic separation*. Miner. Eng. 60, 14-22.

LI, C., SUN, H., BAI, J., LI, L., 2010. *Innovative methodology for comprehensive utilization of iron ore tailings: part 1. The recovery of iron from iron ore tailings using magnetic separation after magnetizing roasting*. J. Hazard. Mater. 174, 71-77.

LI, G. F., HAN, Y. X., GAO, P., SUN, Y. S., 2016. *Enrichment of phosphorus in reduced iron during coal-based reduction of high phosphorus-containing oolitic hematite ore*. Ironmak. Steelmak. 43, 163-170.

LI, W., HAN, Y., LIU, X., SHAN, Y., LI, Y., 2019. *Effect of fluidized magnetizing roasting on iron recovery and transformation of weakly magnetic iron mineral phase in iron tailings*. Physicochem. Probl. Miner. Process. 55, 906-916.

LI, Y. J., WANG, R., HAN, Y. X., WEI, X. C., 2015. *Phase transformation in suspension roasting of oolitic hematite ore*. J. Cent. South Univ. 22, 4560-4565.

NUNES, A. P. L., PINTO, C. L. L., VALADAO, G. E. S., VIANA, P. R. M., 2012. *Floatability studies of wavellite and preliminary results on phosphorus removal from a Brazilian iron ore by froth flotation*. Miner. Eng. 39, 206-212.

SUN, Y., ZHU, X., HAN, Y., LI, Y., 2019. *Green magnetization roasting technology for refractory iron ore using siderite as a reductant*. J. Clean. Prod. 206, 40-50.

SWANN, P. R., TIGHE, N. J., 1977. *High voltage microscopy of the reduction of hematite to magnetite*. Metall. Mater. Trans. B 8, 480-487.

TANG, Z., HAN, Y., GAO, P., LI, E., 2019. *Fluidization characteristics of a u-type reduction chamber in a suspension roaster*. Powder Technol. 345, 64-73.

VYAZOVKIN, S., BURNHAM, A. K., JOSE, M. C., LUIS, A. P., SBIRRAZZUOLI, N., 2011. *ICTAC kinetics commitee recommendations for performing kinetic computations on thermal analysis data*. Thermochim. Acta 520, 1-19.

WANG, Z. H., LI, G. F., SUN, Y. S., HE, M. Z., 2016. *Reduction behavior of hematite in the presence of coke*. Int. J. Min. Met. Mater. 23, 1-8.

YANG, H. F., JING, L. L., ZHANG, B. G., 2011. *Recovery of iron from vanadium tailings with coal-based direct reduction followed by magnetic separation*. J. Hazard. Mater. 185, 1405-1411.

YU, J., HAN, Y., LI, Y., GAO, P., SUN, Y., 2017. *Separation and recovery of iron from a low-grade carbonate-bearing iron ore using magnetizing roasting followed by magnetic separation*. Sep. Sci. Technol. 52, 1768-1774.

YU, J., HAN, Y., LI, Y., GAO, P., 2018a. *Recovery and separation of iron from iron ore using innovative fluidized magnetization roasting and magnetic separation*. J. Min. Metall. B 54, 21-27.

YU, J. W., HAN, Y. X., GAO, P., LI, Y. J., YUAN, S., LI, W. B., 2018b. *An innovative methodology for recycling iron from magnetic preconcentrate of an iron ore tailing*. Physicochem. Probl. Miner. Pro. 54, 668–676.

YU, J. W., HAN, Y. X., GAO, P., LI, Y. J., 2019. *Reductive transformation of Hematite to Magnetite with CO/CO_2 Under Fluidized Bed Conditions*. J. Northeast. Univ. 40, 261–266. (In Chinese)

ZENKOV, V. I., PASICHNYI, V. V., 2010. *Reduction kinetics of iron oxides used for hydrogen production in various gas media*. Powder Metall. Met. C+ 49, 231–237.

ZHANG, X., HAN, Y., SUN, Y, LI, Y., 2019. *Innovative utilization of refractory iron ore via suspension magnetization roasting: a pilot-scale study*. Powder Technol. 352, 16–24.

ZHU, X. R., HAN, Y. X., SUN, Y. S., LI, Y. J., WANG, H. W., 2019. *Siderite as a novel reductant for clean utilization of refractory iron ore*. J. Clean. Prod., https://doi.org/10.1016/j.jclepro.2019.118704.